

EIS analysis on the corrosion resistance of X80 steel under AC interference in simulated soil solution

Zhong Li¹, Baozhuang Sun^{2,*}, Yue Pan², Liang Huang²

¹ Chinese Society of Corrosion and Protection, CSCP, Beijing, 100083, China.

² Corrosion & Protection Center, Key Laboratory of Corrosion and Protection of Ministry of Education, University of Science and Technology Beijing, Beijing 100083, China

*E-mail: sunBAOz9406@163.com

Received: 27 January 2021 / Accepted: 14 March 2021 / Published: 30 April 2021

In this work, the corrosion mechanism of X80 steel under AC interference was studied with electrochemical measurements. The surface potential was monitored at various AC current densities. EIS (electrochemical impedance spectroscopy) measurements were conducted at various AC voltage amplitudes and for various time durations. Variations in the modulus values of the real part and imaginary part were studied. In addition, to simplify the problem, EIS was measured under the effect of various DC potentials. The surface potential was of the same frequency as the AC interference, and the amplitude of the electrode surface potential was linear with the applied current density. As the AC current density increased, the charge transfer resistance decreased due to the acceleration of both the anodic and cathodic processes. When the AC current density reached a certain value, hydrogen and oxygen evolution occurred because the effective Faraday potential exceeded the corresponding critical reaction potential. With an increasing AC time, the charge transfer resistance increased, which was due to the formation of a protective corrosion product film. With the application of low-amplitude AC voltages, there was only a small change in the capacitance of the electric double layer. Nevertheless, with the application of AC voltages at higher amplitudes, the modulus values of the real and imaginary parts of EIS were all less rapid, and the ratio of the imaginary part and real part decreased.

Keywords: AC corrosion; pipeline steel; EIS; charge transfer resistance

1. INTRODUCTION

In recent years, with the rapid development of the world economy, the demand for energy, electricity and electrified railways has continued to grow. Due to geographical location restrictions, many pipelines are buried in parallel or intersect with feeder cables and subway rails, which causes serious stray AC current interference issues. The existence of AC interference causes the corrosion of metal materials to intensify, and severe cases may cause major economic losses and safety accidents [1-3]; in

particular, the susceptibility of pitting corrosion and stress corrosion cracking (SCC) increases [4-15]. Therefore, AC-induced corrosion of pipeline steels cannot be underestimated. There have been many accidents of buried pipeline leakage or explosion caused by AC-induced corrosion in many countries, such as America and Germany. In addition, cathodic protection fails to prevent AC-induced corrosion [13]. Therefore, AC corrosion has already been a hot issue in the field of international corrosion research.

At present, there have been many reports on alternating current corrosion problems. Lalvani [16–18] studied the influence of positive half-waves and negative half-waves on corrosion through an alternating current model and found that the dissolution rate was the highest for full-wave sinusoidal signals and the lowest for negative half-cycle rectified signals. Furthermore, the corrosion rate was generally determined by the DC potential maintained at the anode. Zhang et al. [19] developed a mathematical model related to polarization resistance, double layer capacitance and solution resistance and found that the AC-induced corrosion rate was independent of the DC corrosion rate. Moreover, Sara Goidanich [20] et al. reported that the effect of AC on the corrosion mechanism was mainly embodied in corrosion kinetics and corrosion equilibrium potential. Ono et al. [21] conducted a related study on the alternating current half cycle and Al alloy corrosion and found that when the alternating current was in the anode half cycle, pits formed on the surface of the sample due to the dissolution of the anode. Additionally, when the alternating current was in the negative half cycle, the generated pits were passivated by the anode half cycle. As a result, the nucleation of pitting corrosion exhibited a random distribution. For a pulse current with only a half anode period, the anode pulse current will aggravate the nucleation of pitting corrosion. Therefore, the current induction mechanism for alternating current effects is not uniform, and further research is needed. Previous works [1, 4-19] have shown that corrosion current is related to the AC interference current density and frequency. However, the effect on surface potential remains unsolved. Moreover, although the impact of AC on the electric double layer has been considered, how it acts on the mass transfer process is not considered.

In this work, to investigate the AC influence on the electric double layer of X80 pipeline steel in simulated Korla soil solution, a corrosion mechanism model based on EIS is proposed. The influence of AC interference on the double layer is studied with electrochemical tests. The electric potential and impedance as a function of time are measured with a self-developed experimental device. We expect to provide practical support for AC corrosion evaluation and lay a theoretical foundation for AC corrosion mechanism studies.

2. EXPERIMENTAL

2.1. Materials and solution

The experimental material was hot-rolled X80 steel, and the main chemical components were as follows (in wt.%): C 0.061, Si 0.19, Mn 1.75, P 0.012, S 0.001, Cr 0.033, Ni 0.21, Cu 0.16, Nb 0.045, and an Fe balance.

The experimental solution in this study was a simulated solution of actual soil in Korla, Xinjiang Province, China, which is a typical alkaline soil. The chemical ingredients of the simulated solution are shown in Table 1. The pH of the simulated solution was 9.4.

Table 1. Chemical ingredients of the simulated Korla soil solution (pH=9.4)

Chemicals	NaCl	Na ₂ SO ₄	NaHCO ₃	KNO ₃	MgCl ₂ ·6H ₂ O	CaCl ₂
g/L	3.4945	1.2603	0.146	0.2152	0.3383	0.1221

2.2. Electrochemical setup

The X80 steels were machined with dimensions of 10 mm × 10 mm × 3 mm. The steel electrodes were then coated with epoxy resin keeping an exposed steel surface area of 1 cm². Each group had three parallel samples. The surface of all samples was polished to 1500#, and then acetone and alcohol were used to clean and blow dry. There were at least 3 parallel samples for each experiment. A Gamry reference 3000 electrochemical workstation was used for the experiment. A saturated calomel electrode (SCE) was used as a reference electrode (RE), and a platinum plate was used as a counter electrode (CE). The surface area of the CE was approximately 4 mm². Fig. 1 represents a self-developed device for research on AC-induced corrosion mechanisms. The direct digital synthesis (DDS) function signal generator was used to apply the AC. A graphite sheet was used to form an AC circuit with the specimen. An Owan oscilloscope was used to display the potential under AC interference.

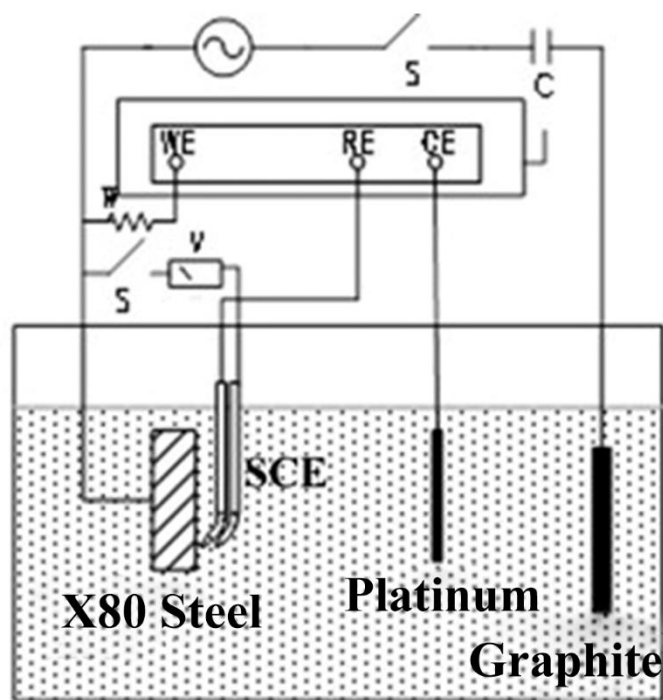


Figure 1. Schematic diagram of the experimental apparatus for electrochemical tests.

2.3 Electrochemical test procedures

Prior to electrochemical tests, the potential difference of two reference electrodes in the test solution was tested through an electrochemical workstation to ensure their error range.

To study the influence of different alternating current densities on the electrode potential of X80 pipeline steel, a 50 Hz alternating current was applied to the sample through the external AT1645-3 function signal generator (Fig. 1), and the current density was 0 A/m², 30 A/m², 60 A/m², 120 A/m², 200 A/m², 300 A/m² and 400A/m². Four hundred sampling points were collected for each cycle change to ensure that the collection was sufficiently accurate. Among them, the capacitor was used to prevent the electrochemical test system from interfering with the AC power supply, and the inductance was used to prevent alternating current interference to the electrochemical test system to ensure that the two circuits were independent of each other. The experiment was carried out at room temperature, and the current value tested during the experiment was the root mean square value.

To study the impact of various AC time durations on the electric double layer, EIS was measured under a 50 Hz AC application with a current density of 60 A/m² for 0 h, 12 h, 24 h, 36 h, and 48 h. In addition, the variations in the imaginary part and real part were studied with EIS measurements at different AC signal voltages. The voltage amplitudes of the excitation signals regulated by the electrochemical workstation were chosen to range from 10 mV to 3000 mV, and the AC frequency was 50 Hz. The test time of each EIS was 600 s

To simplify the AC-induced corrosion mechanism, the influence of different applied DC (direct current) potentials on the electrochemical corrosion of X80 pipeline steel was studied. Different DC potentials ranging from -0.4 V to -1.2 V were applied prior to EIS tests, and then EIS measurements were carried out after the DC was switched off.

EIS measurements were conducted at an AC excitation voltage of 10 mV in the frequency range from 100 kHz to 10 mHz. Prior to EIS tests, specimens were immersed in solution for 30 min until the corrosion potential reached stability. The EIS data were analysed with ZsimpWin software. All experiments were carried out three times to assess the repeatability and accuracy of the data at ambient temperature.

3. RESULTS

3.1 Reference electrode error test

To confirm the error range of the reference electrode used in the experiment, the potential difference between two reference electrodes was measured, and the results are shown in Fig. 2. The error between two reference electrodes is -0.0014 ± 0.0001 V, which is too low to cause an ohmic drop between the solution and WE. Therefore, the error caused by RE can be neglected in this study.

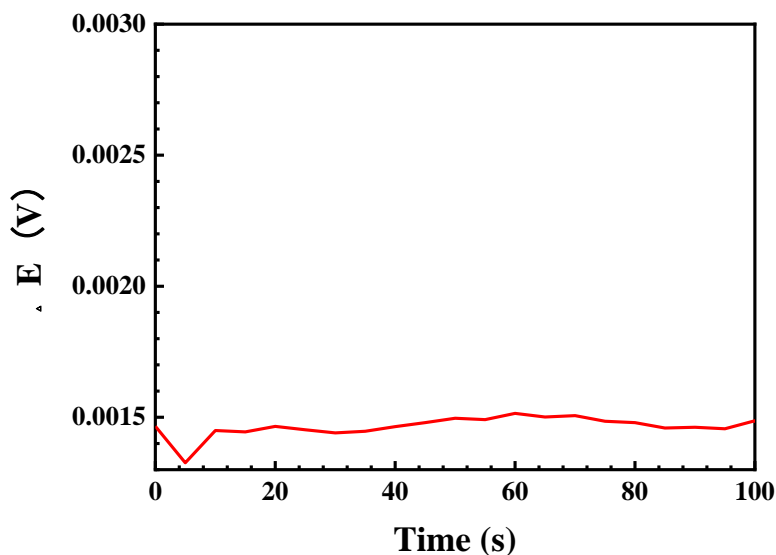


Figure 2. Error range test result for the reference electrodes used in the electrochemical tests.

3.2 Variation of potential of X80 pipeline steel with different AC current density

Fig. 3 shows the potential of X80 pipeline steel at different AC current densities. The figure shows the result of the curve potential change with 100 data points (that is, 2.5 cycles). The variation frequency of the potential is a 50 Hz sine wave curve, which is consistent with the applied AC interference.

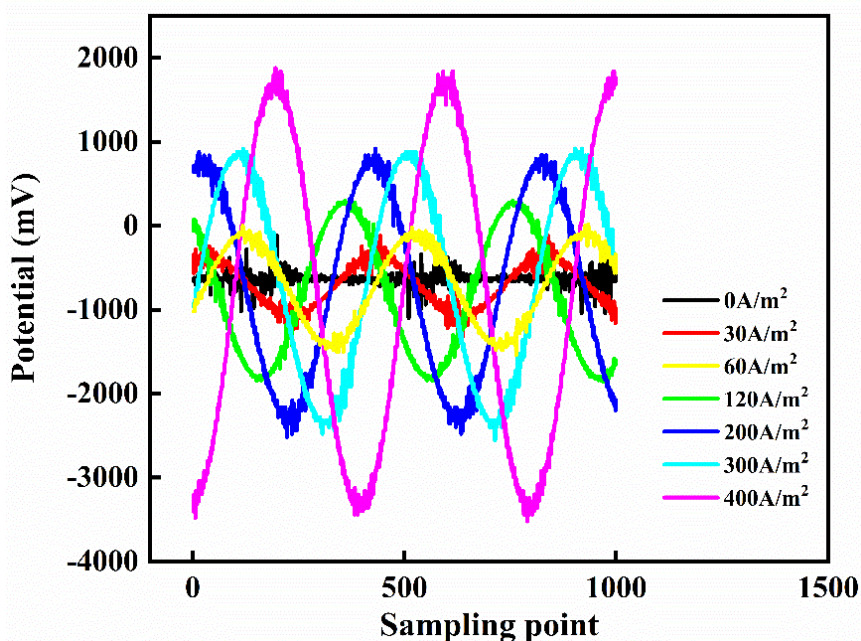


Figure 3. Surface potential of the X80 pipeline steel at different AC current densities in the simulated Korla soil solution

The statistical data were analysed, as shown in Fig. 4. When the AC current density is less than 60 A/m², the mean potential decreases. However, when the AC current density exceeds 60 A/m², the mean potential varies slightly as the AC current density increases and fluctuates at approximately -754 mV. The potential amplitude increases as the AC current density increases and exerts a linear relation with the applied AC current density, which is shown in equation (1).

$$E = 0.0131i \quad (1)$$

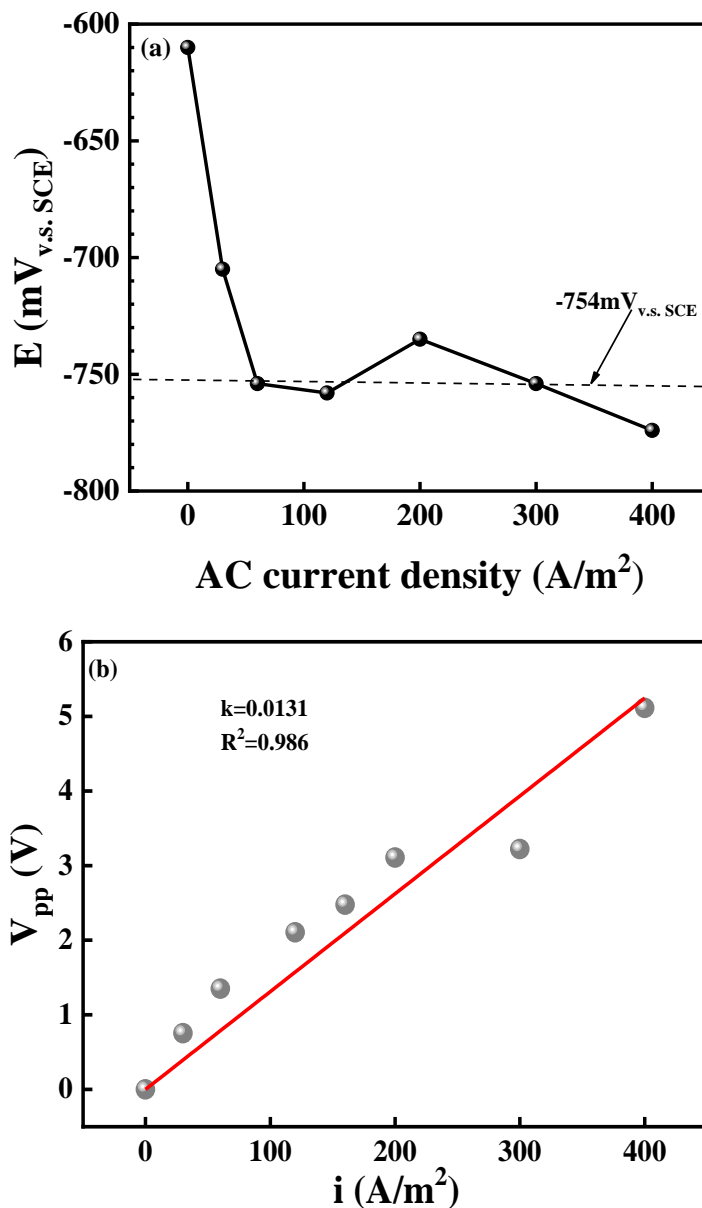


Figure 4. Statistical results of the potential of X80 pipeline steel at different AC current densities in the simulated Korla soil solution: (a) mean potential and (b) potential amplitude

3.3 EIS results of under AC interference with different time

Fig. 5 shows the EIS Nyquist diagram of X80 pipeline steel under 60 A/m² AC interference for

different periods of time. As observed in Fig. 5, the capacitive arc expands as the immersion time increases. The results were fitted and analysed with the equivalent circuit in Fig. 6, where R_s is the solution resistance, Q_{dl} is the constant phase element (CPE) of the electric double layer between the metal and solution, R_t is the charge transfer resistance, Q_f is the CPE of the corrosion product film, and R_f is the resistance of the corrosion product film. At the initial corrosion stage (0 h), the equivalent circuit model is $R_s(Q_{dl}R_t)$, as shown in Fig. 6(a), which is a simple form of bare steel without any corrosion products. As the immersion time increases, the substrate surface is covered with a layer of a corrosion product film. Therefore, two time constants appear, and the equivalent circuit is comprised of $R_s(Q_fR_f(Q_{dl}R_t))$, as shown in Fig. 6(b).

The fitted results of EIS are shown in Table 2. From Table 2, the values of Q_{dl} vary slightly, which characterizes the non-Faradaic process in the electric double layer formed by the matrix and solution, while the charge transfer resistance first decreases and then increases over time. Previous work revealed that the R_t value is inversely related to the electrochemical reaction rate of the anode and can reflect the Faradaic current [5-6]. Therefore, the corrosion rate first increases and then decreases with an increasing immersion time. This may be due to the formation of the corrosion product film: at first, it is loose and thin, and corrosion may be accelerated in weak areas of the film (12-24 h), while in the mid to late corrosion period, the corrosion product film becomes compact, thereby protecting the steel surface against the attack of corrosive ions (36-48 h).

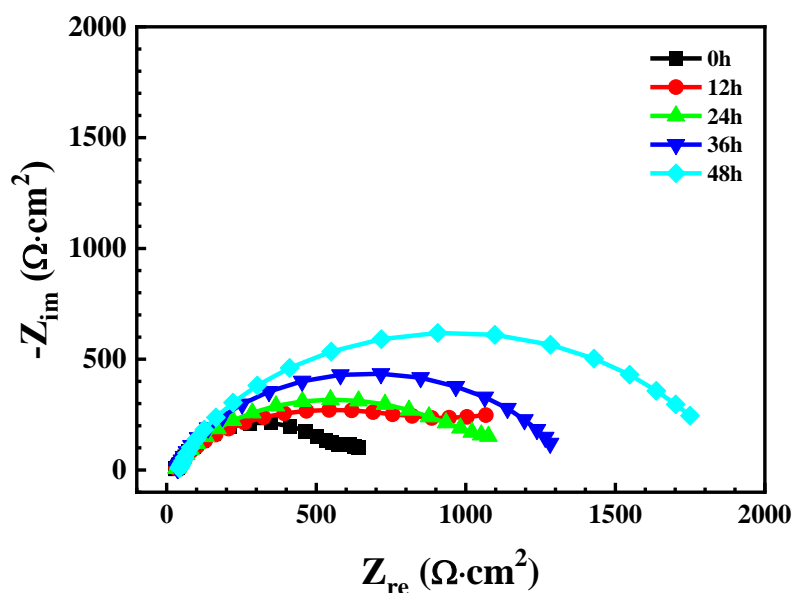


Figure 5. EIS Nyquist diagram of the X80 pipeline steel under 60 A/m² AC interference for different periods of time in the simulated Korla soil solution

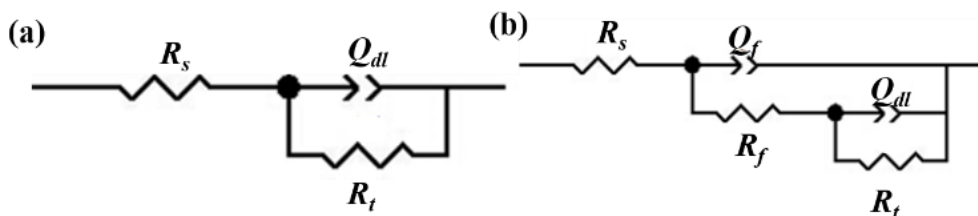


Figure 6. Equivalent circuit model of the EIS results of the X80 steel under 60 A/m² AC interference for different periods of time in the simulated Korla soil solution: (a) 0 h and (b) 12-48 h

Table 2. Fitted EIS results of the X80 pipeline steel under 60 A/m² AC interference for different periods of time in the simulated Korla soil solution

Time	Experimental parameters						
	R_s ($\Omega \cdot \text{cm}^2$)	Q_{dl} ($\Omega^{-1} \cdot \text{cm}^{-2} \cdot \text{s}^n$)	n_{dl}	R_t ($\Omega \cdot \text{cm}^2$)	Q_f ($\Omega^{-1} \cdot \text{cm}^{-2} \cdot \text{s}^n$)	n_f	R_f ($\Omega \cdot \text{cm}^2$)
0h	29.52	0.0006635	0.7721	613.1	/	/	/
12h	28.04	0.0006993	0.7279	546.4	0.004039	0.6042	753.3
24h	30.08	0.0006516	0.8	445.8	0.001722	0.6655	690.1
36h	34.53	0.0007045	0.7493	1167	0.001495	0.9564	149.6
48h	39.57	0.0007584	0.7628	1651	0.001833	0.9036	196.2

3.4 The variation of EIS under different alternating voltage with time

The conventional approach to EIS analysis is to show the imaginary part and the real part in a complex plane with a Nyquist plot. However, it may be inadequate and inapplicable for electrochemical systems with strong AC interference because it fails to display correlations among frequency, testing time, phase angle and low impedance values [20], which are sensitive to the system parameters in unstable electrochemical systems. Therefore, in this part, we studied the variation of the imaginary part and real part to reveal the electrochemical kinetics of the electric double layer, and the values can be calculated as follows:

$$Z_{re} = R_s + \frac{R_t + C\omega^n R_t \cos(\frac{n\pi}{2})}{1 + 2C\omega^n R_t \cos(\frac{n\pi}{2}) + \omega^{2n} C^2 R_t^2} \quad (2)$$

$$Z_{im} = -j \frac{C\omega^n R_t^2 \sin(\frac{n\pi}{2})}{1 + 2C\omega^n R_t \cos(\frac{n\pi}{2}) + \omega^{2n} C^2 R_t^2} \quad (3)$$

$$\tan\phi = \frac{Z_{im}}{Z_{re} - R_s} = \frac{\omega^n C R_t \sin(\frac{n\pi}{2})}{1 + \omega^n C \cos(\frac{n\pi}{2})} \quad (4)$$

Table 3 shows the solution resistance obtained by EIS fitting at different alternating voltages. Fig. 7 shows the variation of the real part exclusive from R_s and the modulus value of the imaginary part of EIS over time at different AC voltage amplitudes. The real part and the modulus value of the imaginary part of the EIS only show minor changes when the AC voltage amplitudes ranges from 10 mV to 100 mV. However, when the AC voltage amplitude exceeds 100 mV and continues to increase, the values of

the real part and the modulus value of the imaginary part of the EIS results decrease sharply.

Fig. 8 shows the values of the phase angle when the AC voltage amplitude varies from 100 mV to 3000 mV. The phase angle value decreases as the AC voltage amplitude increases.

Table 3. Solution resistance values obtained by EIS fitting under different alternating voltages

AC Voltage (mV)	10	30	50	100	500	1000	3000
R_s ($\Omega \cdot \text{cm}^2$)	27.59	28.67	25.36	27.59	28.13	28.82	26.48

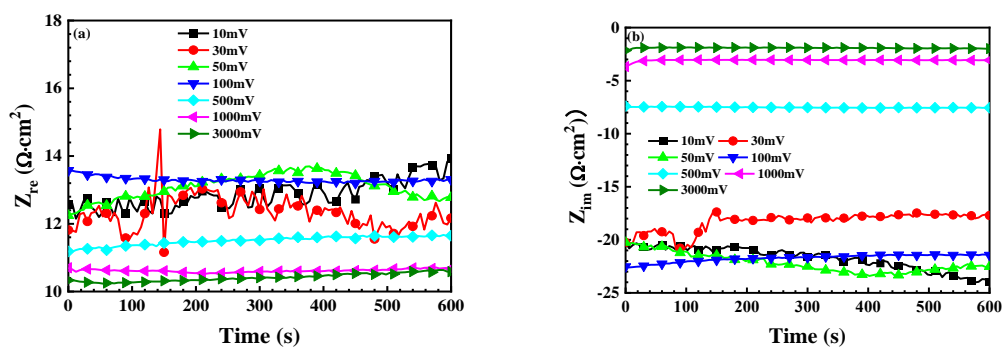


Figure 7. Variation of the EIS results of X80 steel in the simulated Korla soil solution at different applied AC voltage amplitudes over time: (a) real part and (b) imaginary part

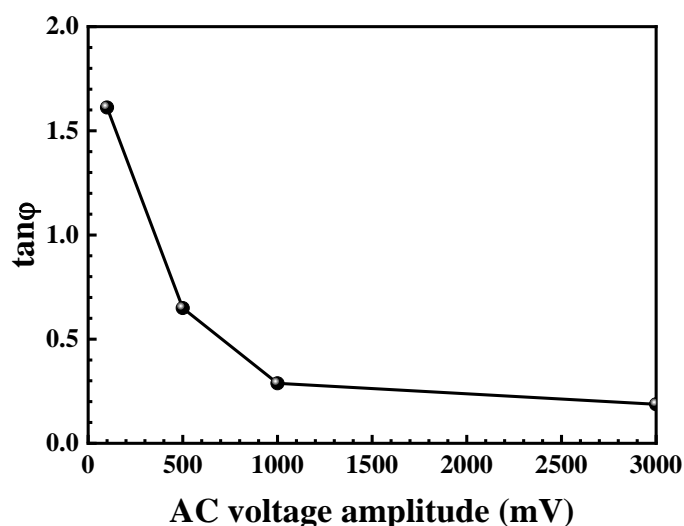


Figure 8. Phase angle values of the EIS results of X80 steel in the simulated Korla soil solution at different applied AC voltage amplitudes

3.5 EIS results under the effect of applied potential

To reveal the AC effect on the electrochemical mechanism, we conducted EIS measurements under the influence of different DC potentials to simplify the question. As shown in Fig. 9. The radius of the capacitive arc of EIS increases when the constant potential varies from -0.4 V to -0.9 V. However, when the constant potential is more negative than -1.0 V, the capacitive arc of EIS decreases rapidly with the continuous negative shift of the DC potential. The EIS results were analysed and fitted with the equivalent circuit in Fig. 6(a), and the fitted results are presented in Table 4. As is also shown in Table 4, the CPE values of the electric double layer only exert a slight change as the applied DC potential shifts from -0.4 V to -1.0 V. However, the values are doubled when the voltages are more negative than -1.0 V, which may be due to the acceleration of the hydrogen evolution.

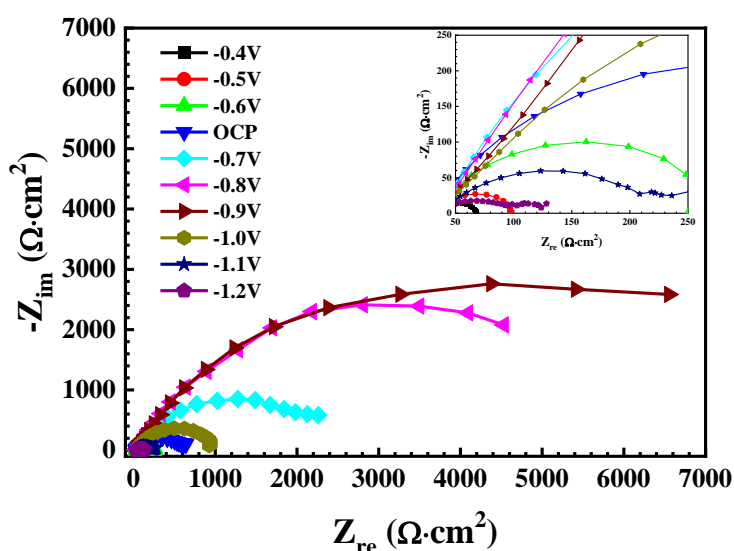


Figure 9. EIS Nyquist plot of the X80 pipeline steel in the simulated Korla soil solution at different applied DC potentials

Table 4. Fitting of the EIS results of X80 pipeline steel in the simulated Korla soil solution at different applied DC potentials

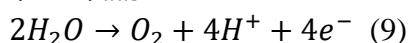
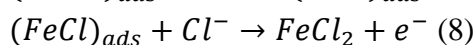
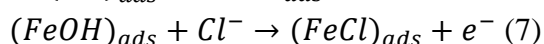
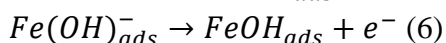
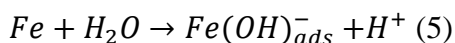
Applied DC potential (V)	Experimental parameters			
	R_s ($\Omega \cdot \text{cm}^2$)	Q_{dl} ($\Omega^{-1} \cdot \text{cm}^{-2} \cdot \text{s}^n$)	n_{dl}	R_t ($\Omega \cdot \text{cm}^2$)
-0.4	30.57	0.0004796	0.7588	38.5
-0.5	31.05	0.0004181	0.8023	70.04
-0.6	31.86	0.000364	0.8408	232.1
OCP	29.52	0.0006635	0.7721	613.1

-0.7	35.26	0.0005467	0.7795	2393
-0.8	34.32	0.0005986	0.7595	7169
-0.9	34.64	0.0005943	0.7376	9094
-1.0	34.74	0.0006692	0.7328	1039
-1.1	33.99	0.001406	0.6387	218.9
-1.2	32.95	0.002886	0.5116	88.57

4. DISCUSSION

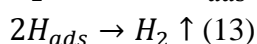
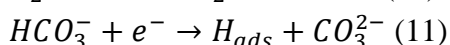
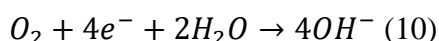
AC interference can be regarded as a long-duration high-frequency cyclic voltammetry process, and it alternates between cathodic and anodic polarization. Therefore, AC application induces cyclic anodic oxidation reactions and cathodic reducing reactions. The effect of AC interference on the electrochemical process consists of two aspects, namely, the non-Faradaic process and Faradaic process [5-6, 21]. The non-Faradaic process refers to the charging and discharging process of capacitance within the electric double layer, which can accelerate mass transfer, while the Faradaic process indicates the electrochemical charge transfer process. The non-Faradaic process only has a minor effect on corrosion, which may be embodied in the slight variation of the CPE values of the electric double layer for various AC interference durations or at various AC current densities. Thus, the effect on the non-Faradaic process can be neglected, and only the impact on the Faraday process is considered.

The electrochemical reactions of X80 steel in an alkaline soil environment involve anodic reactions, cathodic oxygen evolution reactions and hydrogen evolution reactions. The anodic reactions are shown as follows [22]:



AC application can cause an increase in the Faradaic potential. During the positive AC cycle, the anodic dissolution of iron is accelerated. In addition, when the effective potential of the Faradaic process exceeds the oxygen evolution potential, the oxygen evolution reaction can occur, as shown in equation (9). With the presence of an AC, during the AC positive cycle, the AC can promote the anodic dissolution of iron and the evolution of oxygen [23,24].

While the cathodic reactions are as follows.



The cathodic reaction is mainly the oxygen reduction reaction without AC conditions, as shown in the cathodic polarization curve of X80 steel in the simulated Korla soil solution. With the application of an AC, during the AC negative cycle, a negative potential is induced on the steel surface; this negative potential may be over 1 V, exceeding the critical hydrogen evolution potential of X80 steel in the

simulated Korla soil solution [25-28], as shown in Fig. 10. As a consequence, hydrogen evolution is accelerated. Therefore, as the AC current density/voltage amplitude increases to a certain value, the charge transfer resistance decreases drastically, as shown in Table 4.

Regarding the effect of the AC duration on corrosion, Fig. 5 and Table 2 show that after a certain AC interference time, the charge transfer resistance clearly increases. This result may be because in the early period of corrosion, the ongoing electrochemical reaction leads to the formation of the corrosion product film covering the electrode surface, which is a barrier to the corrosive ions and slows the electrochemical reaction. As a consequence, the charge transfer resistance increases. At the same time, when the AC interference is switched off, there is no obvious change in the CPE of the electric double layer. This result shows that the electric double-layer capacitance is not changed after a certain period of AC interference.

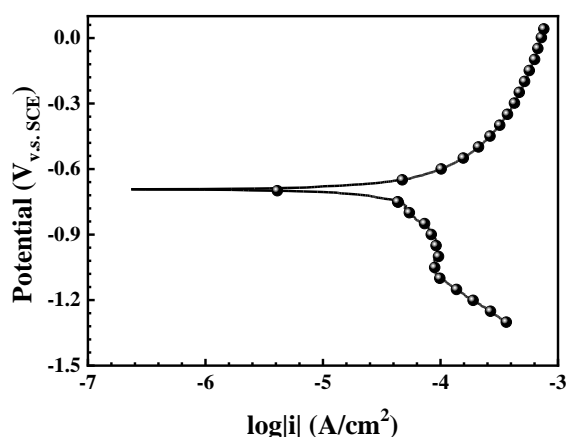


Figure 10. Polarization curve of X80 pipeline steel in the simulated Korla soil solution without applied potential interference

5. CONCLUSIONS

In this work, the effect of AC interference on the electrochemical mechanism of X80 steel in a Korla soil solution was studied through the establishment of an EIS model, laying the foundation for research on the AC-induced corrosion mechanism. The following conclusions were obtained:

(1) The surface potential is of the same frequency as the AC interference, and the amplitude of the electrode surface potential is linear with the applied current density.

(2) As the AC current density increases, the charge transfer resistance decreases due to the acceleration of both the anodic and cathodic processes. When the AC current density reaches a certain value, hydrogen evolution and oxygen evolution occur because the effective Faraday potential exceeds the corresponding critical reaction potential.

(3) With an increasing AC time duration, the charge transfer resistance increases due to the formation of a protective corrosion product film.

(4) With the application of low-amplitude AC voltages, there is only a small change in the capacitance of the electric double layer. Nevertheless, with the application of AC voltages with higher amplitudes, the modulus values of the real and imaginary parts of EIS are all less rapid, and the ratio of the imaginary part and real part decreases.

ACKNOWLEDGMENTS

The authors appreciate the financial support provided by the National Environmental Corrosion Platform of China (NECP)

References

1. Q. Qin, B. Wei, Y. Bai, Q. Fu, J. Xu, C. Sun, C. Wang and Z. Wang, *Eng. Fail. Anal.*, 120 (2021) 105065.
2. S. Goidanich, L. Lazzari and M. Ormellese, *Corros. Sci.*, 52 (2010) 916.
3. S. Muralidharan, D. Kim, T. Ha, J. Bae, Y. Ha, H. Lee and J.D, *Desalination*, 216 (2007) 103.
4. M. Zhu, C. Du, X. Li, Z. Liu, S. Wang, J. Li and D. Zhang, *Electrochim. Acta*, 117 (2014) 351.
5. Y. Pan, Z. Liu, Y. Zhang, X. Li and C. Du, *J. Mater. Eng. Perform.*, 28 (2019) 6931.
6. Q. Liu, W. Wu, Y. Pan, Z. Liu, X. Zhou and X. Li, *Constr. Build. Mater.*, 171 (2018) 622.
7. H. Wan, D. Song, Z. Liu, C. Du, Z. Zeng, Z. Wang, D. Ding and X. Li, *Constr. Build. Mater.*, 154 (2017) 580.
8. H. Wan, D. Song, C. Du, Z. Liu and X. Li, *Bioelectrochemistry*, 127 (2019) 49.
9. K. Tang, *Corros. Sci.*, 152 (2019) 153.
10. D. Kuang and Y. Cheng, *Corros. Sci.*, 85 (2014) 204.
11. L. Wang, X. Wang, Z. Cui, Z. Liu, C. Du and X. Li, *Corros. Sci.*, 86 (2014) 213.
12. Z. Li, C. Li, H. Qian, J. Li, L. Huang and C. Du, *Materials*, 10 (2017) 720.
13. D. Kim, S. Muralidharan, T. Ha, J. Bae, Y. Ha, H. Lee and J. Scantlebury, *Electrochim. Acta*, 51 (2006) 5259.
14. Y. Li, Z. Liu, L. Ke, L. Huang, C. Du and X. Li, *Int. J. Electrochem. Sci.*, 11 (2016) 5021.
15. H. Wan, Z. Liu, C. Du, D. Song and X. Li, *Int. J. Electrochem. Sci.*, 10 (2015) 8437.
16. S. Lalvani and X. Lin, *Corros. Sci.*, 36 (1994) 1039.
17. S. Lalvani and G. Zhang, *Corros. Sci.*, 7 (1995) 1567.
18. S. Lalvani and G. Zhang, *Corros. Sci.*, 37 (1995) 1583.
19. R. Zhang, P. Vairavanathan and S. Lalvani, *Corros. Sci.*, 50 (2008) 1664.
20. C. Wang, W. Li, Y. Wang, X. Yang and S. Xu, *Constr. Build. Mater.*, 247 (2020) 118562.
21. L. Xu, X. Su and Y. Cheng, *Corros. Sci.*, 66 (2013) 263.
22. Z. Liu, C. Du, C. Li, F. Wang and X. Li, *J. Mater. Eng. Perform.*, 22 (2013) 2550.
23. Z. Liu, Z. Cui, X. Li, C. Du and Y. Xing, *Electrochem. Commun.*, 48 (2014) 127.
24. Z. Liu, X. Li and Y. Cheng, *Electrochim. Acta*, 60 (2012) 259.
25. Z. Liu, X. Li and Y. Cheng, *Corros. Sci.*, 55 (2012) 54.
26. S. Goidanich, L. Lazzari and M. Ormellese, *Corros. Sci.*, 52 (2010) 491.
27. S. Ono and H. Habazaki, *Corros. Sci.*, 52 (2010) 2164.
28. W. Qiu, M. Pagano, G. Zhang and S. Lalvani, *Corros. Sci.*, 37 (1995) 97.